A simple Ca^{2+}-imaging approach to neural network analysis in cultured neurons

Zijun Sun[1,2,*] and Thomas C. Südhof[1,2]

[1]Department of Molecular and Cellular Physiology, Stanford University School of Medicine, Stanford, CA 94305, USA.

[2]Howard Hughes Medical Institute, Stanford University School of Medicine, Stanford, CA 94305, USA.

[*]Correspondence to: sunzijun@stanford.edu

Abstract

Ca^{2+}-imaging is a powerful tool to measure neuronal dynamics and network activity. To monitor network-level changes in cultured neurons, neuronal activity is often evoked by electrical or optogenetic stimulation and assessed using multi-electrode arrays or sophisticated imaging. Although such approaches allow detailed network analyses, multi-electrode arrays lack single-cell precision, whereas optical physiology requires advanced instrumentation. Here we developed a simple, stimulation-free protocol with associated Matlab algorithms that enables scalable analyses of spontaneous network activity in cultured human and mouse neurons. The approach allows analysis of overall networks and single-neuron dynamics, and is amenable to scale-up for screening purposes. We validated the new method by assessing human neurons with a heterozygous conditional deletion of Munc18-1, and mouse neurons with homozygous conditional deletions of neurexins. The approach described here enabled identification of differential changes in the amplitudes and synchronicity of neuronal spikes during network activity in these mutant neurons, demonstrating the utility of the approach. Compared with current imaging platforms, our method is simple, scalable, accessible, and easy to implement. It enables quantification of more detailed parameters than multi-electrode arrays, but does not have the resolution and depth of more sophisticated yet labour-intensive analysis methods, such as patch-clamp electrophysiology. The method reported here is scalable for a rapid direct assessment of neuronal function in culture, and can be applied to both human and mouse neurons. Thus, the method can serve as a basis for phenotypical analysis of mutations and for drug discovery efforts.

Key words

Ca^{2+}-imaging, network activity, synaptic transmission, synaptic connectivity, automated image analysis, human neurons

1. INTRODUCTION

Ca^{2+}-imaging provides a wide range of applications in neuroscience because it allows monitoring large populations of neurons *in vivo* and in culture[1]. In culture, neurons exhibit two primary activity modes, sparse spiking of individual neurons and synchronous firing of multiple neurons in networks. Depending on the developmental stage of cultured neurons, Ca^{2+}-imaging typically reveals some spontaneous firing of neurons[2-4]. As neurons form mature neural networks, synchronous firing of neurons via network activity increases in parallel with the synapse density, and can be visualized by Ca^{2+}-imaging[4]. The properties of network activity in cultured neurons depends not only on the extent of synaptic communication between neurons, but also on the electrical properties and the axonal and dendritic development of these neurons as well as on their cellular state[2-5]. Therefore, network firing of neurons represents a proxy for a broad range of neuronal properties, including their developmental maturity, synaptic connectivity, and signalling status.

One challenge in measuring the network activity in cultured neurons, however, is that the synchronicity happens stochastically and depends on the culture quality (density, age etc)[3,6]. As a result induction of network activity often requires external stimulation, such as using electrodes or optogenetics to induce responses[7]. Recently, imaging-based platforms have been developed using sophisticated all-optical electrophysiology, which allows network-level analyses by applying optical stimuli and monitoring individual cells[8,9]. A major advantage of external stimulation in network analyses is that external stimulation enables observation of how synchronized firing is induced, i.e., provides causality. A drawback is that the delivery of stimuli introduces additional complexity to the imaging setup, for example implementation of electrodes or installation of optical lightguides for stimulation. Moreover, variations in the stimulus efficacy may produce variable responses[10]. Another approach to stimulating network activity in cultured neurons is by applying an activating pharmacological agent. This approach is particularly useful for neurons derived from human embryonic stem (ES) or induced pluripotent stem (iPS) cells that may be difficult to analyse because they are generally less mature than neurons in primary cultures and exhibit less spontaneous network activity[8]. However, pharmacologically induced responses may differ from more physiologically spontaneous responses[11].

The abovementioned issues underscore the need for a less sophisticated Ca^{2+}-imaging approach that can analyse sparse and synchronous neuronal activity, and that could aid studies in human stem cell-derived neurons. Here, we describe a simple Ca^{2+}-imaging protocol that elevates the spontaneous activity of human neurons in a stimulation-free manner and provides an analysis pipeline that quantifies network activity and single-neuron dynamics. We offer procedures for the culture and imaging of human and mouse neurons, step-wise illustrations of the analysis pipeline, and interpretations of the results. Network activity of cultured human neurons was robustly induced in the optimised Ca^{2+}-imaging conditions, rendering it suitable for the study of neuronal mutations. We validated the sensitivity and robustness of this approach by testing mutants that were previous shown to exhibit defects in synaptic transmission and connectivity[12,13].

Ca^{2+}-imaging monitors intracellular Ca^{2+}-fluxes that are thought to be caused by neuronal depolarization and action potential firing[14]. The fluorescence signal of GCaMP-type Ca^{2+}-indicators needs to be further analysed to infer the underlying neuronal activity by extracting the features of Ca^{2+} spikes[1]. In the image analysis algorithms we wrote, various parameters were quantified including amplitude, synchronicity rate, and the oscillatory signatures of Ca^{2+}-waveforms via frequency density analyses. The goal of this protocol is to establish an easily accessible and reproducible Ca^{2+}-imaging approach that can be scaled up for mutagenesis analysis or drug screening purpose.

2. Materials and Methods

2.1 Generation of Ngn2-induced human neuron expressing GCaMP Ca^{2+}-indicators

We used a co-culture system of induced human neurons (iN cells) with mouse glia, which provides a supporting layer and factors required for neuronal survival, dendritic arborization, and synapse formation[15-17] (**Fig. 1A**). Human neurons were trans-differentiated from H1 ES cells that were cultured on Matrigel-coated 6-well plate according to the manufacturers' protocols (Corning), and maintained in culture medium containing mTeSR plus basal medium and 5 x supplement (Stem Cell Technologies). Thiazovivin (2 μM, BioVision) was supplemented into the seeding media. Induction of iN cells was performed via lentiviral delivery of the tetracycline transactivator (rtTA) and tetracycline-responsive (*TetO*)-driving Ngn2 as described[15]. H1 ES cells were infected at the same time with lentiviruses expressing GCaMP6m under control of the human synapsin-1 promoter. Lentiviruses were produced in HEK293T cells by calcium phosphate transfection[18]. After lentiviral transduction, cells were maintained in DMEM/F12 medium supplemented with BDNF (10 ng/ml, PeproTech), laminin (0.2 μg/ml, Invitrogen), human NT-3 (10 ng/ml, PeproTech), N2 supplement (ThermoFisher Scientific), Doxycycline (2 μg/ml, Sigma-Aldrich), and non-essential amino acid solution (ThermoFisher Scientific) with daily media changes. Puromycin (1 μg/ml, InvivoGen) was added for two days from DIV2. On DIV4, the developing human iN cells were dissociated with Accutase (Innovative Cell Technologies) and seeded at a density of $1.8\text{-}2\times10^5$ cells/coverslip onto overnight Matrigel-coated coverslips (in 24-well plates) containing mouse glia that had been plated 24-48 hrs previously. After DIV4, the mixed neuron/glia cultures were maintained in Neurobasal medium (ThermoFisher Scientific) supplemented with B27 Supplement (ThermoFisher Scientific) and Glutamax (ThermoFisher Scientific), with a weekly change of half of the medium. On DIV6, Ara-C (Sigma-Aldrich) was added to the culture medium (2 μM final concentration). On DIV10, fetal bovine serum (ATLANTA Biological; final concentration = 2-3%) were added to the culture medium. Ca^{2+}-imaging was performed at DIV35-40 (**Fig. 1A**).

2.2 Generation of mouse cortical primary neuron with GCaMP expression

Cortical primary neurons from newborn triple neurexin-1/2/3 conditional KO mice[13] were seeded on Matrigel-coated coverslips in a 24-well plate in MEM medium (ThermoFisher Scientific). On DIV2, the medium was changed to Neurobasal medium containing 2 μM AraC. On DIV3, half of the medium was exchanged, and the cells were infected with two lentiviruses that encoded (1) GCaMP6m and (2) ΔCre-P2A-mCherry or Cre-P2A-mCherry (all driven by the human synapsin promoter). Cultures were maintained through DIV14-16, when Ca^{2+}-imaging was performed.

2.3 *Ca^{2+}-imaging*

Coverslips were gently washed twice in modified Tyrode solution (25 mM HEPES (Invitrogen), 150 mM NaCl, 5 mM KCl, 1 mM $MgCl_2$, 10 mM glucose, 2 mM $CaCl_2$, pH 7.2–7.4, pre-warmed to 37 °C), and placed into a glass-bottom 12-well plate (Cellvis) containing Ca^{2+}-imaging buffer (25 mM HEPES, 150 mM NaCl, 8 mM KCl, 1 mM $MgCl_2$, 10 mM glucose, 4 mM $CaCl_2$, pH to 7.2–7.4). After 1-2 min equilibration, Ca^{2+}-imaging was performed on an inverted epi-fluorescence microscope (Nikon EclipseTS2R, DS-Qi2 digital camera) with the 488 nm filter at room temperature. GCaMP6m fluorescence was recorded for 2-3 min at a frame rate of 4-10 frames/s. Approximately 800-3000 time-lapse images depending on the frame rate (536x536 pixel resolution, 14-bit grayscale depth for human and mouse cultures) were acquired at a 1 x digital zoom using either a 10x or 20x objective. Acquisition time of each frame can vary between 0.01-0.1s, depending on the camera

used for detection and the exposure time subjected to the brightness of GCaMP expression; long-term recording can cause photobleaching and phototoxicity. Per coverslip, 2-3 fields were imaged and a minimal of 3 coverslips were recorded for each biological batch. For each batch, all images were acquired using the same light intensity and exposure time. Time-lapse imaging was performed in a field of view (FOV) containing confluent neuron populations with non-overlapping soma.

2.4 *Image pre-processing*

Time-lapse image files were converted to *.tiff /.tif* format using ImageJ (https://imagej.nih.gov/ij/). Quantifications were performed using home-written Matlab functions and scripts included in the **Appendix A-B**. To determine the network activity of the neuronal culture based on the synchronous firing of cell population in the entire FOV, follow section 3.2; to determine the single-neuron activity based on the amplitude and frequency, follow section 3.3 and 3.4.

2.5 Statistical analyses

Matlab (MathWorks) was used to process images and quantifications from time-lapse tiff files. Data were exported from Matlab to *.csv* files which were imported for plotting into R software (http://www.r-project.org, version 1.2.5001; R packages ggplot2, tidyverse, lubridate). All *P* values were calculated using Student's *t*-test with $P < 0.05$ considered significant, unless otherwise stated.

3. Results

3.1 Imaging of neurons and image analysis

Human neurons expressing GCaMP6m and co-cultured with mouse glia (**Fig. 1A**) were imaged in a standard epi-fluorescence microscope, and the GCaMP6m fluorescence signal was recorded as a function of time. Regions of interests (ROIs) containing the neurons to be analysed were manually selected from the images using the Matlab function *GCAMP_multiROI.*m (**Appendix B. 1**), which extracts the raw intensity signal of GCaMP6m from the ROIs. The function first projects the stack to its maximum intensity image to allow a user to find and select a neuron. The ROI is a squared box defined by selecting the center of the neuron soma, and the size of the ROI can be specified in the function according to the acquisition resolution (see **Appendix A** for detailed instructions and example of variable definitions) (**Fig. 1B**). After selection of all desired ROIs, the traces of the GCaMP6m fluorescence intensity per ROI over time were generated. The intensity profile was automatically saved into a *.mat* file named after the image name in a folder automatically created. The raw data is in the matrix *ROI_intensity1,* which can be found by loading the *.mat* file in the command window, and each column is one cell while the row is the time-course. To plot the raw intensity of the Ca^{2+} signal, load the *ROI_intensity1* matrix generated from the above step and run the script *Raw_intensity.m* (**Appendix B. 2**). This will return a figure showing all traces (traces panel in **Fig. 1B**).

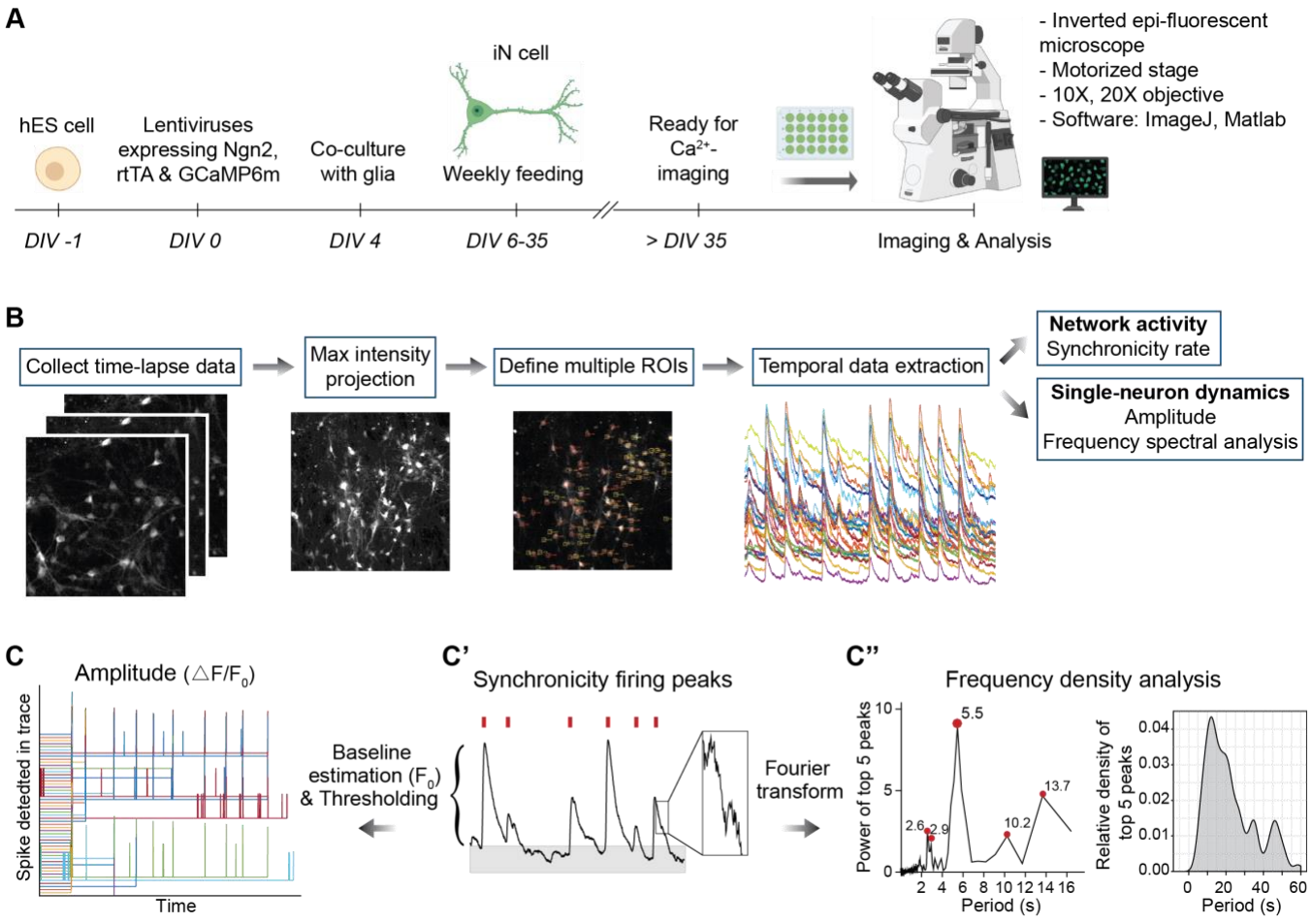

Fig. 1. Ca^{2+}-imaging and analysis workflow. (**A**) Culturing and imaging pipeline of induced human neurons (iN cells). At 0 days *in vitro* (DIV0), human ES or iPS cells were infected with lentiviruses expressing Ngn2 (from the tetO promoter activated by co-expressed rtTA) and with lentiviruses expressing GCaMP6m (under the synapsin promoter). At DIV4, cells were co-cultured with mouse glia. Cells were maintained by weekly feeding up to DIV35 for maturation of Ca^{2+}-imaging. For image acquisition and analysis, an inverted epi-fluorescent microscope with a digital camera and a 10x or 20x objective connected to a PC or Macintosh equipped with image analysis software ImageJ and Matlab are required.

A motorized microscope stage with robotic timing of imaging is optional. (**B**) Image processing and analysis protocol. First, time-lapse images are 'stacked' to provide a maximal intensity projection. Then, ROIs are manually selected centering on the neuronal soma (the X-Y coordinates are indicated next to each ROI box). Finally, raw intensity values of the Ca^{2+} signal are extracted from selected ROIs. Network activity is quantified via the synchronicity rate, while single-neuron dynamics are quantified via the Ca^{2+} signal amplitude and frequency density. (**C**) Example figure showing spike detection for amplitude normalization. The peaks were detected after thresholding based on the estimation of the baseline fluorescence level (F_0), and the amplitude was normalized to $\Delta F/F_0$. (**C'**) Illustration of an averaged Ca^{2+} trace induced by synchronous spikes indicated by short red lines. The inset shows oscillations at different sizes within the trace. (**C''**) Example graphs of the frequency density analysis. Left panel, example graph of the power-spectrum analysis extracting top 5 peaks by fast Fourier transform analysis of a single neuron's activity. Right panel, example of the density from the frequency of top 5 peaks compiled from a population of neurons.

3.2 Analysis of network activity by inducing synchronicity

In cultured Ngn2-induced neurons trans-differentiated from ES cells, individual neurons exhibited occasional spontaneous Ca^{2+}-spikes (**Fig. 2A-A'**), but synchronous firing of two or more neurons was rare (**Fig. 2A-A', C**). Therefore we elevated neuronal firing by increasing the concentrations of Ca^{2+} and of K^+ in the imaging solution to 4 mM and 8 mM, respectively. Under this condition, frequent synchronous firing was observed in cultured neurons (**Fig. 2B-B', D, Table 1**). When we manually counted the peaks during synchronous firing, we found that the synchronicity rate was not high (typically below 10/min with this condition; **Fig. 2D**). The synchronicity rate is defined as the number of synchronous peaks per minute (synchronous Ca^{2+} spikes/min). Since the signal-to-noise ratio is large, peak counts and measurements of the synchronicity rate can easily be automated using appropriate algorithms (see below). Ngn2-induced human neurons are composed exclusively of excitatory neurons[15]. As a result, addition of CNQX (10 μM), an antagonist of AMPA-type glutamate receptors, to the neurons suppressed network activity, although some isolated Ca^{2+} spikes could still be observed in the presence of CNQX (**Fig. 2E**). Treatment of the cultured neurons with tetrodotoxin (TTX; 1μM), a Na^+-channel blocker, also abolished synchronous activity of neurons, as evidenced by a complete loss of synchronous Ca^{2+} spikes, which would be expected for network activity driven by action potential firing (**Fig. 2F**). Note that TTX also ablates all sparse spontaneous Ca^{2+} spike firing, supporting the notion that spontaneous non-synchronous Ca^{2+} spikes also depend on action potential firing (**Fig. 2F**).

3.3 Spike detection and amplitude normalization

Here, we adopted a semi-automated approach that used a built-in Matlab function for spike detection but manually set the baseline determination range. We identified spikes using a threshold of 2-6 standard deviations (s.d.) above the baseline variation[19] (see **Table 1** for trouble-shooting advice). The baseline was determined as the averaged intensity of the minimal fluorescence intensity (without spiking) from the first 400 frames, middle 200 frames and the last 400 frames within each trace, to compensate for photobleaching. The amplitude and the frequency of Ca^{2+} signals are common parameters quantified during Ca^{2+} imaging[20] (**Fig. 1C**). To compute the amplitude, we loaded the *ROI_intensity1* matrix generated in the above step and ran the script *Amplitude_ddF0.m* (**Appendix B. 3**). The normalized amplitude is thereby calculated as the change of fluorescence (delta F, ΔF) over the baseline fluorescence (F_0) of Ca^{2+} spikes (DF/F_0)[1]. Running this program gives two outputs: a plot of detected spikes (**Fig. 1C**) and a plot of Ca^{2+} traces after normalization (e.g. **Fig. 2C-F**). The normalized amplitude of individual Ca^{2+} spikes as a function of time is saved to the *dFF0* matrix, in which the columns consist cells while the row is the time-course. The averaged amplitude of all spikes detected in an entire time course is saved to the *deltaFtoF0* matrix.

3.4 Single-neuron frequency density analysis and thresholding

Besides the amplitude of Ca^{2+} spikes, their frequency represents a fundamental parameter of neuronal Ca^{2+} signalling[20-22]. Because individual Ca^{2+} transients during network activity are produced by underlying oscillations at different frequencies and are dependent on both meaningful information and noise, we performed frequency density analyses (**Fig. 1C''**). We first extracted the frequency components from the raw trace by power-spectrum density quantifications using fast Fourier transform (FFT)[23-26] in the function *FFT_TOP5peaks.m* (**Appendix B. 4**, see **Appendix A** for variable specifications). This function plots the five frequencies with the highest power for a given individual neuron (e.g., **left panel**, **Fig. 1C''**) and saves the value to the matrix *freq_period_pow_perc.mat*, which can be exported for the density quantification. This method is useful when little information can be directly deduced from temporal data, and provides a straightforward, quantitative understanding of the frequency composition of the temporal dynamics of Ca^{2+} signals in an unbiased manner[24,26]. The relative density graph was plotted from as many cells as analysed from the single-neuron analysis by *FFT_TOP5peaks.m.* It is important to collect a sufficiently large sample size to get a fair density distribution. The example in **Fig. 1C''** show that the most prominent oscillation period of Ca^{2+} spikes present in this neuronal population is around 10 s. For statistical analysis, the density data can be binned in a histogram and compared between specific periods. Because the time-lapse data used for the power-spectrum analysis were taken for 2 min, oscillation periods above 60 s were considered overflow from the FFT calculation and not plotted. In addition, we performed thresholding using the Ca^{2+} signals recorded in TTX-treated cultures as a baseline to exclude non-action potential related oscillation wavelengths. TTX-treated neurons exhibited only Ca^{2+} signals with a periodicity above 11 s/cycle (**Fig. 2G**). Thus, oscillation periods above 11 s were excluded from all analyses (**Fig. 2G-G'**).

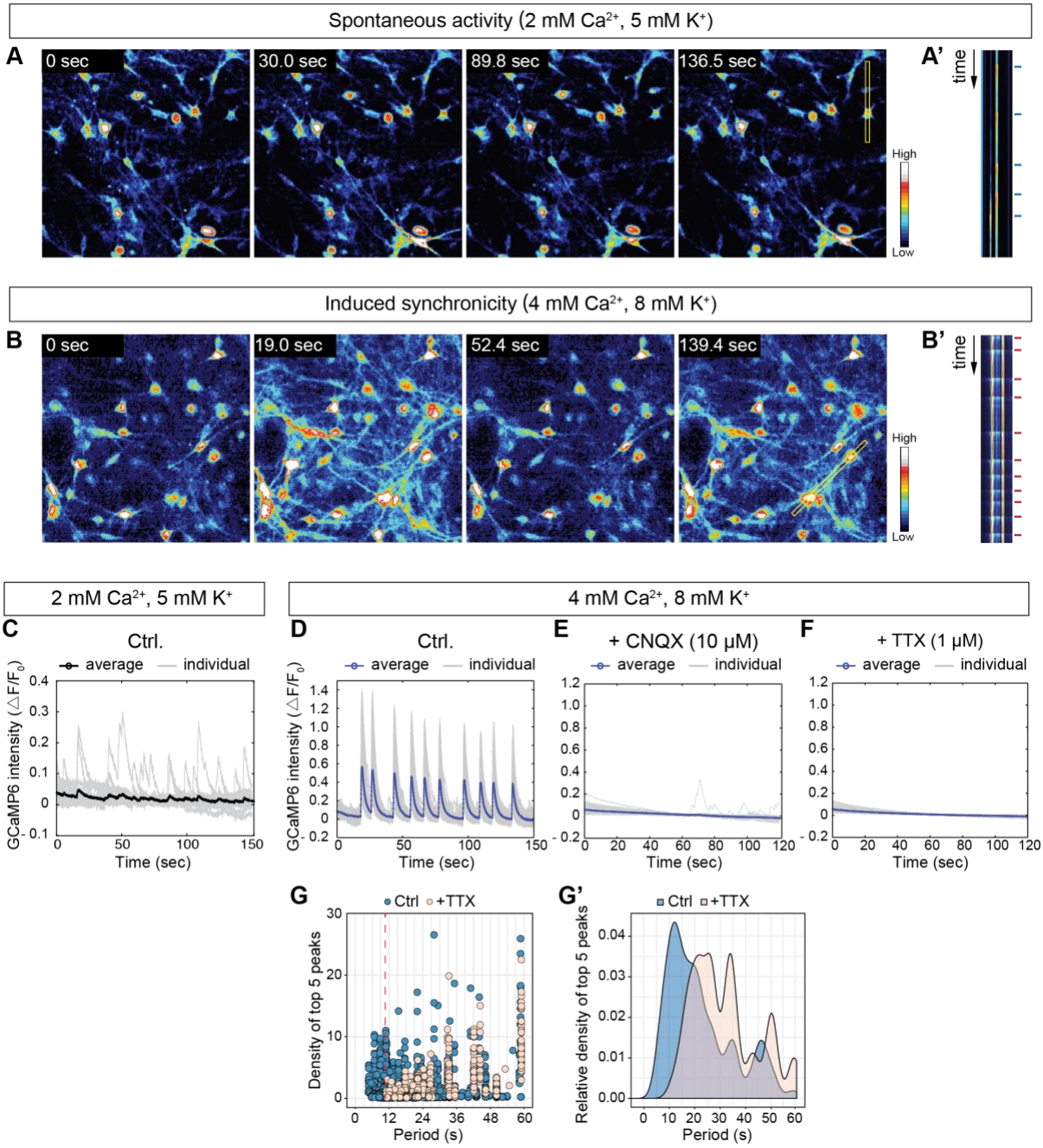

Fig. 2. Analysis illustration of network activity and thresholding. (**A** & **A'**) Representative time-lapse images of the spontaneous activity of human neurons expressing GCaMP6m monitored in modified Tyrode solution (**A**). The kymograph (**A'**; represents two neurons are from the yellow box in the rightmost panel in **A**) for the first 90 s of recording showed non-synchronous spikes, as indicated by blue lines. (**B** & **B'**) Same as **A** & **A**', but for neurons examined in modified Tyrode solution with an increased Ca_{2+} and K_{+} concentration. In the kymograph (**B'**), synchronous spikes are indicated by red lines. (**C**) Ca_{2+} signal traces plotted from (**A**). No significant synchronous peaks are observed from the averaged intensity (black line), but individual Ca_{2+} spikes are present (light-grey lines). (**D**) Ca_{2+} traces plotted from (**B**). Synchronous peaks are observed in the averaged intensity (blue line; light-grey lines indicate individual Ca_{2+} traces). (**E** & **F**) Representative Ca_{2+} traces monitored in neurons in modified Tyrode solution with an increased Ca_{2+} and K_{+} concentration and in the presence of 10 μM CNQX (**E**) or 1 μM TTX (**F**). (**G** & **G'**) Thresholding for frequency density analysis by TTX treatment (**G**, individual data points; **G'**, relative density plot). The 11 s period frequency was used as thresholding filter as indicated by the red dotted line in **G**. 776 neurons were quantified for the control condition (Ctrl) and 274 neurons from TTX condition for **G** & **G'**.

Table 1 | Troubleshooting table.

Section	Problem	Solution

3.1	No synchronous firing observed but neurons fire individually	1) Density of neurons in culture affects their connectivity; increase density if necessary. 2) Neuronal maturity and glia quality. Make sure the glia cover most of the bottom layer. Glia should not exceed more than 2 months before iN co-culture.
3.2	Error in Matlab: Index exceeds matrix dimensions	The threshold is not appropriately set. Typically it is 2-6 x s.d. of the baseline, but may vary to different data. Adjust in the code *Amplitude_ddF0.m* (**Appendix B. 3**), line 10.

3.5 Analysis of conditional KO of munc18-1 in human iN

To validate the Ca^{2+} imaging approach described above, we analysed a previously characterized mutation affecting synaptic transmission, the heterozygous conditional knockout (cKO) of Munc18-1 (human gene symbol: *STXBP1*)[27]. Munc18-1 is a central component of the synaptic vesicle fusion machinery (reviewed in reference[28]). We imaged human neurons transdifferentiated from H1 ES cells carrying the conditional Munc18-1 deletion with expression of either an inactive mutant Cre (□Cre, control) or Cre (to induce the deletion) in addition to GCaMP6m. Specifically, Munc18-1 cKO H1 cells were co-infected on DIV0 with lentiviruses expressing Cre-P2A-mCherry or □Cre-P2A-mCherry in addition to lentiviruses expressing Ngn2, rtTA and GCaMP6m. We then performed Ca^{2+} imaging on the resulting neurons at DIV35-40, which revealed a dramatic change in Ca^{2+} spiking and synchronous network activity in Munc18-1 mutant neurons (**Fig. 3A, B**). Immunoblotting confirmed that Cre-expressing Munc18-1 cKO neurons exhibited a reduction of ~60% in Munc18-1 protein levels (**Fig. 3C**).

Analysis of the neuronal Ca^{2+} spikes demonstrated that the heterozygous Munc18-1 deletion caused a ~50% suppression of neuronal network activity quantified as the synchronous firing rate (**Fig. 3D**). In addition, the deletion produced a ~20% decrease in Ca^{2+} signal amplitude (**Fig. 3E**). Because mutant and control neurons might exhibit a qualitative difference in network oscillation in addition to the quantitative changes in synchronous firing rate and Ca^{2+} signal amplitude (**Fig. 3F**), we binned the frequency density data into two groups: below 9 s and between 9-11 s. We then calculated the ratio of the relative density of spikes (percentage of spikes with periods of <9 s versus spikes with periods of 9-11 s) for mutant and control cells. This analysis revealed that mutant Munc18-1 cKO neurons exhibited fewer spikes at higher frequencies (periods of <9 s) compared to controls, indicating a reduced firing activity in the “faster” (<9 s) frequency spectrum (**Fig. 3F, G**). These results were in agreement with the previous findings that the heterozygous loss of Munc18-1 in human neurons causes a major decrease in synaptic strength as evidenced by a highly reduced evoked EPSC amplitude and a decreased mEPSC frequency[27].

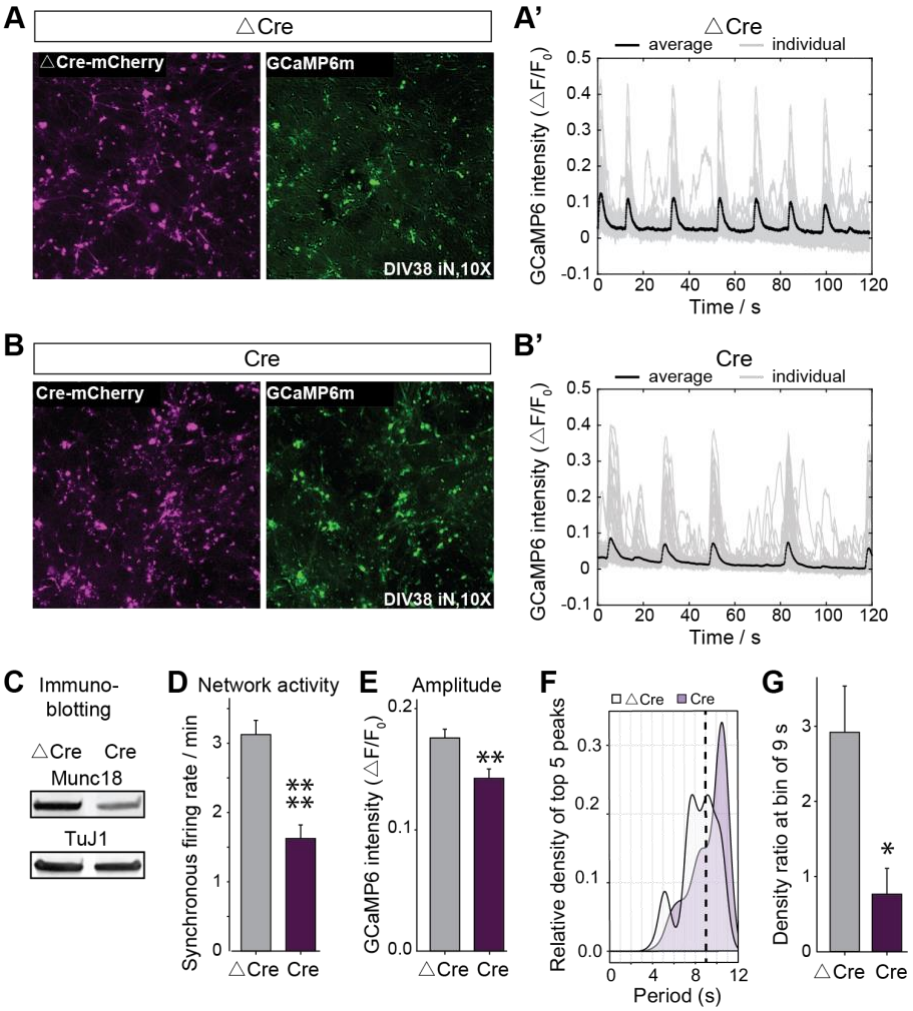

Fig. 3. Analysis of network and neuronal activities in munc18-1 cKO human neurons. (**A** & **B**) Representative images of the mCherry (left) and the GCaMP6m signal (right) observed in heterozygous human Munc18-1 cKO neurons expressing □Cre (control) or Cre (deletion) as analysed at DIV38 with 10x objective. (**A'** & **B'**) Individual (thin lines) and averaged Ca2+ signal traces, monitored as the GCaMP6m fluorescence intensity, recorded in experiments whose representative images are shown on the left. (**C**) Immunoblots of control (△Cre) and heterozygous mutant neurons (Cre). (**D**) Quantification of network activity as the synchronicity firing rate for control and heterozygous mutant neurons. 2-3 FOVs from 3 biological batches (n = 8 FOVs/batch) were recorded for control and mutant human neurons each. (**E**) Quantification of the normalized amplitude by calculating $\triangle F/F_0$ of GCaMP6m intensity for control and heterozygous mutant neurons (n = 689 and 981 neurons from control and Munc18-1-mutant neurons from 3 biological replicates). (**F**) Density plot of the frequency of top 5 peaks for control and heterozygous mutant neurons. Dotted line indicates the bin region at 9 s for the subsequent statistical analysis. (**G**) Quantification of the frequency density ratio for control and heterozygous mutant neurons (n = 186 and 180 neurons from control and Munc18-1-mutant neurons from 3 biological replicates for **F** and **G**). Data in **D**, **E**, **G** represent mean ± SEM. Student's *t*-tests were used for all groups (*, p<0.05; **, p<0.01; ****, p<0.0001).

3.6 Analysis of conditional triple KO of neurexin in mouse cortical neurons

In a second experiment, we aimed to validate our Ca^{2+} imaging approach in mouse neurons, using mice with a conditional deletion of all neurexins, referred to as pan-neurexin deletion. Neurexins are presynaptic adhesion molecules that act as a key regulators of synapse properties[29]. We cultured cortical neurons from newborn triple neurexin-1/2/3 cKO mice that we reported earlier[13]. Deletion of all three neurexins has no effect on synapse numbers, but causes profound changes in the efficacy of synaptic transmission[13,30]. We infected the cultured cortical neurons at DIV3 with lentiviruses expressing GCaMP6m and □Cre (control) or Cre (deletion), and analysed the neurons by Ca^{2+} imaging at DIV14-16 as described in section 2.2 (**Fig. 4A**). The pan-neurexin deletion significantly

decreased neuronal network activity, as shown by a decreased synchronous firing rate (**Fig. 4B-D**). However, the pan-neurexin deletion also cause a significant, somewhat paradoxical increase of the amplitude of the Ca^{2+} spikes (**Fig. 4B'', C''**, **E**). The frequency density plot uncovered a slight shift of the firing frequency from below 7.7 s to longer period lengths in neurexin-deficient neurons compared to control (**Fig. 4F**). We therefore calculated the ratio of the densities of spikes with <7.7 s periods versus spikes with 7.7-11 s periods. This analysis revealed an increase of Ca^{2+} spikes with longer periods (e.g., low frequencies) in the neurexin-deficient neurons compared with control (**Fig. 4G**).

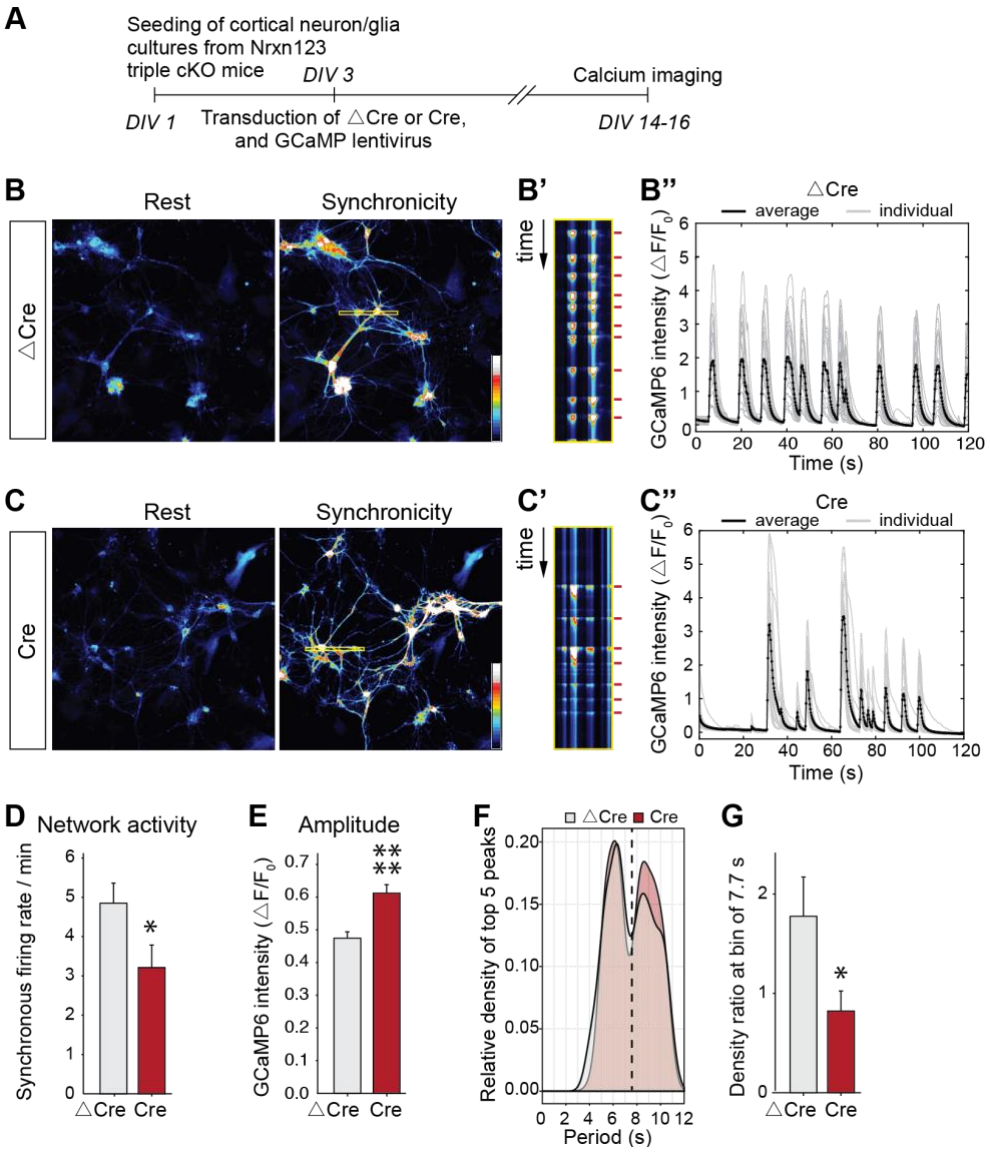

Fig. 4. Analysis of neuronal network activity in cortical neurons cultured from triple neurexin-1/2/3 cKO mice. (**A**) Experimental strategy for culturing and imaging cortical neurons from triple neurexin-1/2/3 cKO mice. (**B-B''** &**C-C''**) Ca^{2+} imaging analysis of network activity of control neurons (**B-B''**; triple neurexin-1/2/3 cKO neurons expressing □Cre) and neurexin-deficient neurons (**C-C''**; triple neurexin-1/2/3 cKO neurons expressing Cre). Representative images of Ca^{2+} signals monitored in neurons in standard medium (Rest) and in medium containing 4 mM Ca^{2+} and 8 mM K^{+} (Synchronicity) are shown on the left (**B** & **C**); kymographs of the neurons included in the yellow boxes in the 'Synchronicity' images are depicted in the middle, with red lines marking Ca^{2+} spikes (**B'** & **C'**); and Ca^{2+} traces on the right (**B''** & **C''**; thin lines depict individual neurons, and thick lines averages). (**D**) Quantification of the synchronous firing rate as a measure of network activity in control and neurexin-deficient neurons (n = 20 FOVs for control and 19 FOVs for neurexin-deficient neurons from 4 biological batches). (**E**) Quantification of the normalized amplitude by calculating $\triangle F/F_0$ of GCaMP intensity for Ctrl and mutant neurons (n = 1476 control and 1282 neurexin-deficient neurons from 4 biological batches). (**F**) Density plot of the frequency of top 5 peaks for control and neurexin-deficient neurons. Dotted line indicates the bin region at 7.7 s for the following statistical analysis. (**G**) Quantification of the frequency density ratio for control and neurexin-deficient neurons (n = 279 control and 249 neurexin-deficient neurons from 4

biological batches). Data in **D**, **E**, **G** represent means ± SEM. Student's t-tests were used for all groups (*, $p<0.05$; ****, $p<0.0001$).

4. Discussion

In this study we developed a Ca^{2+} imaging approach that enables functional analysis of cultured neurons based on network activity and single-neuron Ca^{2+} dynamics. The mechanisms underlying neuronal network activity have been studied extensively by patch-clamp electrophysiology, which provides an exquisite amount of precise information but is only suitable for low-throughput applications. We induced synchronous network activity in human and mouse neurons by raising the ambient Ca^{2+} and K^{+} concentrations, which made analysis of network activity possible. Because the network activity depends, among others, on the synaptic connectivity, the analysis of network activity can be used to survey mutants that exhibit potential synaptic phenotypes. Indeed, we validated our Ca^{2+} imaging approach with human and mouse neurons that carry conditional synaptic mutations, human heterozygous Munc18-1 cKO neurons and mouse homozygous triple neurexin-1/2/3 cKO neurons. Our data confirmed that the simple Ca^{2+} imaging approach we described is not only capable of robustly detecting mutant phenotypes, but can also differentiate between different types of phenotypes (**Fig. 3, 4**). Although the conclusions derived from such analyses of Ca^{2+} signalling and network activity in mutant neurons are generic and cannot be interpreted with regard to a specific mechanism, these conclusions provide direct assessments of network activity and represent a useful readout for analysis of mutations or pharmacological agents.

The Ca^{2+} imaging approach developed here is relatively simple. Moreover, this approach can be readily expanded to monitor additional parameters. For example, we quantified the Ca^{2+} signal from the soma of a neuron, the activity of which comes from hundreds of synaptic inputs. To measure Ca^{2+} signals directly at the level of synapses, GCaMPs could be targeted to pre- or postsynaptic specializations by fusion to synaptophysin[11] or PSD95[31], respectively.

Furthermore, we adopted a semi-automated image analysis approach. For the manual part, we allowed users to select interested neurons to be analysed (**Fig. 1b**) and define the threshold of baseline for spike detection (**Fig. 1c**), while the data extraction and computation of the amplitude, frequencies are automatic. The advantage of a fully-automated object selection and thresholding is that it would minimize researcher bias and enable medium-to-high throughput data profiling. The drawback of thresholding using a fixed value is it is a trade-off between including more weaker but real signals and not introducing too much background noises. In the protocol, we analysed the network activity by the frequency of the synchronicity peaks, yet there might be cases where percentage of synchronous neurons decreased while the synchronicity frequency remained[3]. This prompt for more in-depth descriptor such as the percentage of the synchronous neurons or synchronous amplitude etc. Although we also computed the amplitude and the frequency density quantifications of individual neuron to infer single-neuron dynamics, many excellent Ca^{2+} imaging analysis packages have increased the number of features that can be rapidly extracted from cells, allowing for a more comprehensive evaluation of neuronal activity at scale[12,32-35]. The increasing size of the imaging datasets demands that the analysis automated, ultimately towards standardization and automation to leverage phenotypic assays especially in human neuronal models and can also be exploited in the drug screening context for neurodegenerative or neuropsychiatric disorders[1-3,5].

Credit author statement

Z.S. and T.C.S. jointly conceived the experiments, Z.S. performed the experiments, and Z.S. and T.C.S. analysed the results and wrote the manuscript.

Declaration of Competing Interests

None.

Acknowledgements

The authors would like to thank Drs. Jinye Dai, Christopher Patzke, Steve Wilson, Kathlyn Gan, and Yang Yang for advice and reagents. This work was supported by a grant from the NIMH (U19 MH104172, to T.C.S.).

References

1. Grienberger C, Konnerth A. Imaging calcium in neurons. *Neuron* 2012; **73**(5): 862-85.
2. Verstraelen P, Pintelon I, Nuydens R, Cornelissen F, Meert T, Timmermans JP. Pharmacological characterization of cultivated neuronal networks: relevance to synaptogenesis and synaptic connectivity. *Cell Mol Neurobiol* 2014; **34**(5): 757-76.
3. Verschuuren M, Verstraelen P, Garcia-Diaz Barriga G, et al. High-throughput microscopy exposes a pharmacological window in which dual leucine zipper kinase inhibition preserves neuronal network connectivity. *Acta Neuropathol Commun* 2019; **7**(1): 93.
4. Brewer GJ, Boehler MD, Pearson RA, DeMaris AA, Ide AN, Wheeler BC. Neuron network activity scales exponentially with synapse density. *J Neural Eng* 2009; **6**(1): 014001.
5. Verstraelen P, Van Dyck M, Verschuuren M, et al. Image-Based Profiling of Synaptic Connectivity in Primary Neuronal Cell Culture. *Front Neurosci* 2018; **12**: 389.
6. Virdee JK, Saro G, Fouillet A, et al. A high-throughput model for investigating neuronal function and synaptic transmission in cultured neuronal networks. *Sci Rep* 2017; **7**(1): 14498.
7. Wardill TJ, Chen TW, Schreiter ER, et al. A neuron-based screening platform for optimizing genetically-encoded calcium indicators. *PLoS One* 2013; **8**(10): e77728.
8. Fan LZ, Nehme R, Adam Y, et al. All-optical synaptic electrophysiology probes mechanism of ketamine-induced disinhibition. *Nat Methods* 2018; **15**(10): 823-31.
9. Williams LA, Joshi V, Murphy M, et al. Scalable Measurements of Intrinsic Excitability in Human iPS Cell-Derived Excitatory Neurons Using All-Optical Electrophysiology. *Neurochem Res* 2019; **44**(3): 714-25.
10. Peled ES, Newman ZL, Isacoff EY. Evoked and spontaneous transmission favored by distinct sets of synapses. *Curr Biol* 2014; **24**(5): 484-93.
11. Reese AL, Kavalali ET. Single synapse evaluation of the postsynaptic NMDA receptors targeted by evoked and spontaneous neurotransmission. *Elife* 2016; **5**.
12. Patel TP, Man K, Firestein BL, Meaney DF. Automated quantification of neuronal networks and single-cell calcium dynamics using calcium imaging. *J Neurosci Methods* 2015; **243**: 26-38.
13. Chen LY, Jiang M, Zhang B, Gokce O, Sudhof TC. Conditional Deletion of All Neurexins Defines Diversity of Essential Synaptic Organizer Functions for Neurexins. *Neuron* 2017; **94**(3): 611-25 e4.
14. Smetters D, Majewska A, Yuste R. Detecting action potentials in neuronal populations with calcium imaging. *Methods* 1999; **18**(2): 215-21.
15. Zhang Y, Pak C, Han Y, et al. Rapid single-step induction of functional neurons from human pluripotent stem cells. *Neuron* 2013; **78**(5): 785-98.

16. Huang YA, Zhou B, Wernig M, Sudhof TC. ApoE2, ApoE3, and ApoE4 Differentially Stimulate APP Transcription and Abeta Secretion. *Cell* 2017; **168**(3): 427-41 e21.
17. Huang YA, Zhou B, Nabet AM, Wernig M, Sudhof TC. Differential Signaling Mediated by ApoE2, ApoE3, and ApoE4 in Human Neurons Parallels Alzheimer's Disease Risk. *J Neurosci* 2019; **39**(37): 7408-27.
18. Tsetsenis T. Monitoring Synapses Via Trans-Synaptic GFP Complementation. *Methods Mol Biol* 2017; **1538**: 45-52.
19. Piatkevich KD, Bensussen S, Tseng HA, et al. Population imaging of neural activity in awake behaving mice. *Nature* 2019; **574**(7778): 413-7.
20. Mackay L, Mikolajewicz N, Komarova SV, Khadra A. Systematic Characterization of Dynamic Parameters of Intracellular Calcium Signals. *Front Physiol* 2016; **7**: 525.
21. Adachi Y, Kindzelskii AL, Ohno N, Yadomae T, Petty HR. Amplitude and frequency modulation of metabolic signals in leukocytes: synergistic role of IFN-gamma in IL-6- and IL-2-mediated cell activation. *J Immunol* 1999; **163**(8): 4367-74.
22. Clapham DE. Calcium signaling. *Cell* 2007; **131**(6): 1047-58.
23. Uhlen P. Spectral analysis of calcium oscillations. *Sci STKE* 2004; **2004**(258): pl15.
24. Bortone D, Polleux F. KCC2 expression promotes the termination of cortical interneuron migration in a voltage-sensitive calcium-dependent manner. *Neuron* 2009; **62**(1): 53-71.
25. Wu M, Wu X, De Camilli P. Calcium oscillations-coupled conversion of actin travelling waves to standing oscillations. *Proc Natl Acad Sci U S A* 2013; **110**(4): 1339-44.
26. Akin O, Bajar BT, Keles MF, Frye MA, Zipursky SL. Cell-type-Specific Patterned Stimulus-Independent Neuronal Activity in the Drosophila Visual System during Synapse Formation. *Neuron* 2019; **101**(5): 894-904 e5.
27. Patzke C, Han Y, Covy J, et al. Analysis of conditional heterozygous STXBP1 mutations in human neurons. *J Clin Invest* 2015; **125**(9): 3560-71.
28. Sudhof TC. Neurotransmitter release: the last millisecond in the life of a synaptic vesicle. *Neuron* 2013; **80**(3): 675-90.
29. Sudhof TC. Synaptic Neurexin Complexes: A Molecular Code for the Logic of Neural Circuits. *Cell* 2017; **171**(4): 745-69.
30. Luo F, Sclip A, Jiang M, Sudhof TC. Neurexins cluster Ca(2+) channels within the presynaptic active zone. *EMBO J* 2020; **39**(7): e103208.
31. Dreosti E, Odermatt B, Dorostkar MM, Lagnado L. A genetically encoded reporter of synaptic activity in vivo. *Nat Methods* 2009; **6**(12): 883-9.
32. Kaifosh P, Zaremba JD, Danielson NB, Losonczy A. SIMA: Python software for analysis of dynamic fluorescence imaging data. *Front Neuroinform* 2014; **8**: 80.
33. Giovannucci A, Friedrich J, Gunn P, et al. CaImAn an open source tool for scalable calcium imaging data analysis. *Elife* 2019; **8**.
34. Oh J, Lee C, Kaang BK. Imaging and analysis of genetically encoded calcium indicators linking neural circuits and behaviors. *Korean J Physiol Pharmacol* 2019; **23**(4): 237-49.
35. Zhou P, Resendez SL, Rodriguez-Romaguera J, et al. Efficient and accurate extraction of in vivo calcium signals from microendoscopic video data. *Elife* 2018; **7**.